Video Article

# Fast Imaging Technique to Study Drop Impact Dynamics of Non-Newtonian Fluids

Qin Xu[1,2], Ivo Peters[2], Sam Wilken[1,2], Eric Brown[3], Heinrich Jaeger[1,2]

[1]Department of Physics, The University of Chicago

[2]James Franck Institute, The University of Chicago

[3]Department of Mechanical Engineering and Materials Science, Yale University

Correspondence to: Heinrich Jaeger at h-jaeger@uchicago.edu

URL: http://www.jove.com/video/51249
DOI: doi:10.3791/51249

Keywords: Physics, Issue 85, fluid mechanics, fast camera, dense suspension, liquid metal, drop impact, splashing

Date Published: 3/5/2014

Citation: Xu, Q., Peters, I., Wilken, S., Brown, E., Jaeger, H. Fast Imaging Technique to Study Drop Impact Dynamics of Non-Newtonian Fluids. *J. Vis. Exp.* (85), e51249, doi:10.3791/51249 (2014).

## Abstract

In the field of fluid mechanics, many dynamical processes not only occur over a very short time interval but also require high spatial resolution for detailed observation, scenarios that make it challenging to observe with conventional imaging systems. One of these is the drop impact of liquids, which usually happens within one tenth of millisecond. To tackle this challenge, a fast imaging technique is introduced that combines a high-speed camera (capable of up to one million frames per second) with a macro lens with long working distance to bring the spatial resolution of the image down to 10 μm/pixel. The imaging technique enables precise measurement of relevant fluid dynamic quantities, such as the flow field, the spreading distance and the splashing speed, from analysis of the recorded video. To demonstrate the capabilities of this visualization system, the impact dynamics when droplets of non-Newtonian fluids impinge on a flat hard surface are characterized. Two situations are considered: for oxidized liquid metal droplets we focus on the spreading behavior, and for densely packed suspensions we determine the onset of splashing. More generally, the combination of high temporal and spatial imaging resolution introduced here offers advantages for studying fast dynamics across a wide range of microscale phenomena.

## Video Link

The video component of this article can be found at http://www.jove.com/video/51249/

## Introduction

Drop impact onto a solid surface is a key process in many applications involving electronic fabrication[1], spray coating[2], and additive manufacturing using inkjet printing[3,4], where a precise control of drop spreading and splashing is desired. However, direct observation of drop impact is technically challenging for two reasons. First, it is an intricate dynamic process that occurs within a timescale too short (~100 μsec) to be imaged easily by conventional imaging systems, such as optical microscopes and DSLR cameras. Flash photography can of course image much faster, but does not allow for continuous recording, as required for detailed analysis of the evolution with time. Second, the length scale induced by impact instabilities can be as small as 10 μm [5]. Therefore, to quantitatively study the impact process a system that combines ultrafast imaging along with reasonably high spatial resolution is often desired. In the absence of such system, early work on droplet impact focused mostly on the global geometric deformation after impact[6-8], but was unable to gather information about the early time, nonequilibrium processes associated with impact, such as the onset of splashing. Recent advances in CMOS high speed videography of fluids[9,12] have pushed the frame rate up to one million fps and exposure times down below 1 μsec. Furthermore, newly developed CCD imaging techniques can push the frame rate well above one million fps[9-12]. Spatial resolution on the other hand, can be increased to the order of 1 μm/pixel using magnifying lenses[12]. As a consequence, it has become possible to explore in unprecedented detail the influence of a wide range of physical parameters on various stages of drop impact and to systematically compare experiment and theory[5,13-16]. For instance, the splashing transition in Newtonian fluids was found to be set by atmosphere pressure[5], while the intrinsic rheology decides the spreading dynamics of yield-stress fluids[17].

Here a simple yet powerful fast imaging technique is introduced and applied to study the impact dynamics of two types of non-Newtonian fluids: liquid metals and densely packed suspensions. With exposure to air, essentially all liquid metals (except mercury) will spontaneously develop an oxide skin on their surface. Mechanically, the skin is found to alter effective surface tension and wetting ability of the metals[18]. In a previous paper[15], several of the authors studied the spreading process quantitatively and were able to explain how the skin effect influences the impact dynamics, especially the scaling of the maximum spreading radius with impact parameters. Since liquid metal has high surface reflectivity, careful adjustment of the lighting is required in the imaging. Suspensions are composed of small particles in a liquid. Even for simple Newtonian liquids, the addition of particles results in non-Newtonian behavior, which becomes especially pronounced in dense suspensions, *i.e.* at high volume fraction of suspended particles. Particularly, the onset of splashing when a suspension droplet hits a smooth, hard surface was studied in the previous work[16]. Both liquid-particle and inter-particle interactions can change the splashing behavior significantly from what might be expected from simple liquids. To track particles as small as 80 μm in these experiments a high spatial resolution is needed.

 

A combination of various technical requirements such as high temporal and spatial resolution, plus the capability for observing impacts both from the side and from below, can all be satisfied with the imaging setup described here. By following a standard protocol, described below, the impact dynamics can be investigated in a controlled fashion, as shown explicitly for spreading and splashing behavior.

## Protocol

# 1. Fast Imaging Setup (See Figure 1)

1. Start by setting up a vertical track along which a container filled with the fluid to be studied can be freely moved to adjust the impact velocity. The fluid leaves the bottom of the container through a nozzle and then enters free fall. For this work the falling height was varied from 1-200 cm to give an impact velocity $V_0$ = (0.4-6.3)±0.15 m/sec.
2. Construct and mount a frame to hold the horizontal impact plane, typically a glass plate, under which an inclined reflective mirror is positioned for visualizing the drop impact from the bottom.
3. Place a clean and smooth glass plate onto the holder. Make sure the plate is leveled horizontally.
4. Mount a syringe pump onto the vertical track.
5. For liquid metal impact, place a transparent paper diffuser behind the nozzle for side-view imaging. At the same time, attach a white opaque paper above the syringe pump to generate reflection for bottom viewing (see **Figure 1**). Then, locate the light source behind the nozzle.
6. For dense suspension impact, no diffuser is needed. Instead, just place the light source in front of the imaging plane.
7. Select the macro lens with an appropriate focal length for desired magnification and optical working distance. Then, connect the lens to the camera.
8. Mount the camera onto a tripod and adjust the height of camera according to the imaging perspective (side or bottom).

# 2. Sample Preparation

1. **Preparation of oxidized liquid metal**
    1. Store Gallium-Indium Eutectic (eGaIn) in a sealed container. Since its melting temperature is about 15 °C, eGaIn stays in a liquid state at room temperature.
    2. Use a pipette to extract 3 ml eGaIn from the container and extrude it onto an acrylic plate. Wait 30 min for the sample to be fully oxidized in air. As a consequence, a thin layer of wrinkled oxidized skin completely covers the sample surface.
    3. Use hydrochloric acid (HCl; "CAUTION") of different concentrations to prewash the eGaIn sample and to control the surface oxidation. Specifically, shear the sample, while it is in the acid bath, at 60 $sec^{-1}$ shear rate with a rheometer. After 10 min of shear, the level of surface oxidation in the sample reaches equilibrium, set by the HCl concentration[15,18].
    4. After this prewash, use a plastic syringe with a steel nozzle tip to extract eGaIn from the bath.
    5. Mount the syringe onto the syringe pump and be ready for the experiment.

2. **Preparation of dense suspensions**
    1. Cut off the end of a commercial syringe (4.5 mm or 2.3 mm in radius) and use it as cylindrical tube for dispensing the dense suspension.
    2. Pull back the piston and fill the syringe with water all the way to the open end, making sure there is no air bubble entrained.
    3. Put spherical $ZrO_2$ or glass beads into the syringe. With the sedimentation of particles, water will spill out from the nozzle. Fill the syringe with particles all the way to the open end. The suspension will jam under gravity.
    4. Use a razor blade to remove extra wetted particles from the top to keep that end flat.
    5. Flip over the nozzle and mount it onto the syringe pump. Surface tension will prevent the particles from falling out[16].

# 3. Calibration

Before collecting videos, the parameters of the imaging device have to be set and lighting alignment has to be completed. Also, the spatial resolution needs to be calibrated.

1. Start the syringe pump at a speed of 20 ml/hr to push out the fluid (liquid metal or suspension) from the nozzle.
2. Wait for the fluid to detach from the syringe, form a drop and fall off to make a test impact onto the glass substrate.
3. Adjust the camera position, including its vertical position and imaging orientation, to find the splat in the computer monitor that connects to the camera. Modify the working distance to arrange the image to be in the focal plane when the reproduction ratio of the lens is fixed at 1:1.
4. Vary the aperture size, exposure time and lighting angle to obtain the best image quality when the frame rate is high enough (>6,000 fps). **Figure 2(a)** shows typical images taken by the camera for both liquid eGaIn and a dense suspension.
5. Place a ruler in the field of view (see **Figure 2(b)**) and calculate the spatial resolution by counting how many pixels fit across 1 cm. Make sure there is no difference in resolution between horizontal and vertical directions.
6. Follow a 3-step process to measure the packing fraction of dense suspension drop:
    1. Measure the mass of the entire splat right after impact (*e.g.* by letting the drop fall into a measuring cup that can be weighed accurately).
    2. Then, evaporate all solvent with a heater and weigh the splat again to obtain the particle mass.
    3. Calculate the volume of particles and liquid to get the packing fraction. Typically, this volume fraction should be around 60%.

7. According to the observation direction (bottom or side), position the camera appropriately. In particular, put the camera next to the substrate for the side view or on the same level of the reflective mirror for bottom imaging.

## 4. Video Recording and Data Acquisition

1. After imaging calibration, restart the syringe pump. At the same time, open the camera controlling software to monitor the impact process.
2. Set the post-triggering frame numbers at roughly half of the video length. Watch carefully when the drop starts to form and manually trigger the camera at the moment when drop detaches from the nozzle. Perform a few practice tests before data recording.
3. After the data is recorded, trim down the video to the portion containing the impact and save the videos as image sequences for analysis.

## 5. Image Post-processing and Analysis

1. Use a boundary detection method to locate the moving front of liquid eGaIn as it spreads, which corresponds to a sharp transition in the average pixel value (see **Figures 3(a-b)**).
2. From both bottom and side images, determine the splashing onset of dense suspension.
3. Perform particle-tracking algorithms to obtain traces of individual particles that escaped from the splat (see **Figure 3(c)**). Then, calculate the ejecting velocity from such trajectories (**Figure 3(d)**).

## Representative Results

The fast imaging technique can be used to quantify spreading and splashing for various impact scenarios. **Figure 4(a)**, for instance, shows typical impact image sequences for liquid eGaIn with different oxide skin strength. By ejecting eGaIn from the same nozzle and at the same falling height, droplets with reproducible impact velocity $V_0$ = 1.02±0.12 m/sec and radius $R_0$ = 6.25±0.10 mm were generated. The left column shows the impact of an air-oxidized eGaIn drop not prewashed in acid. A long tail at the top end of the drop is formed when the fluid detaches from the nozzle. Differing from ordinary liquids, the oxide skin prevents the fluid from freely relaxing the surface energy, so this nonspherical geometry is kept unchanged during the falling stage. After the impact occurs, a thin liquid metal sheet (lamella) expands rapidly along the smooth substrate. Washing the samples in acid reduces the oxide and weakens the skin effect. The middle and right columns in **Figure 4(a)** show images of drops prewashed in 0.01 M and 0.2 M HCl, respectively. When the acid becomes strong enough to fully eliminate any observable skin effect, eGaIn shows no difference in spreading behavior from ordinary liquids (right column).

In order to characterize the radial expansion after impact, the spreading factor can be defined as $P_m = R_0 / R_m$, where the maximum spreading radius is $R_m$. The scaling behavior of $P_m$ under different oxidation conditions is plotted in **Figure 4(b)** in a conventional way for Newtonian fluids, where Re is the Reynolds number and We* is an effective Weber number that accounts for surface stress induced by the induced skin. Here, the Reynolds number and the effective Weber number for eGaIn are defined on the scale of the entire drop. Particularly, $Re = 2V_0R_0/v$ where v is the kinematic viscosity and $We^* = 2\rho V_0^2 R_0/\sigma_{eff}$ with ρ as the liquid density and $\sigma_{eff}$ as the effective surface tension. [15] The data nicely collapse onto the classical scaling[6]. This suggests that the spreading of oxidized eGaIn conforms to the energy balance argument used to explain spreading for Newtonian fluids, as long as the elastic energy stored in the skin is accounted for. Generally, no splashing of eGaIn is observed since the surface tension (>400 mN/m) is much larger than in ordinary liquids.

For dense suspensions, the experiments focused on the splash onset. A nonviscous liquid was used as the solvent so that the particle Reynolds number $Re_p$ was always larger than 400. In this regime, viscous dissipation is negligible compared to inertial effects. **Figure 5** shows the splashing phase diagram for different particle densities $\rho_p$ and radii $r_p$. Since the single particle dynamics dominates the impact, both Reynolds number and Weber number are defined on the single particle scale. Namely, $Re_p = V_0R_p/v$ and $We_p = \rho_pV_0^2 R_p/\sigma$, where $R_p$ is the particle radius. Here, changing the impact velocity varies the particle Weber number $We_p$. For each point in the plot, the experiment was repeated for 10 times. The red hollow circles are the cases where splash is always found, and the solid blue dots correspond to the situation when no splash is found. The open green squares, however, indicate the scenarios when both splash and no splash are observed in the 10 repeats. In all cases, the transition to splashing happens at the same value of $We_p \approx 14$. This is consistent with an argument that the particle-based Weber number is the relevant parameter for the splash onset[16]. The insets show representative images of splash and no splash situations. By comparing the results to the splashing transition of Newtonian fluids, a distinctive difference emerges. Conventionally, splashing onset for Newtonian liquids is set by the dimensionless quantity $K=We^{1/2}Re^{1/4}$, where Weber number, We, and Reynolds number, Re, are defined for the entire drop[7]. However, by adding particles into the liquid, an extra length scale, the particle size, is introduced into the system. As a result, in the case where suspensions are as dense as the jamming point, the dynamics of individual particle determines the splashing onset.

One of the distinctive features of dense suspensions is the lace-like structure formed in the aftermath of impact (**Figure 6(a)**). In order to characterize this new type of instability, the area of the opened holes is quantified through imaging analysis. First, the velocity distribution in the spreading layer can be obtained by using Particle Image Velocimetry (PIV). Then, the yellow rings in **Figure 6(a)** are defined with particle Weber number $We_p$ = 10, 75, and 920, which all expand radially with time. By imaging analysis, the area of the holes and the total area between each ring are obtained as $S_{hole}$ and $S_0$, respectively. The ratio of $S_{hole}$ to $S_0$ is plotted against time in **Figure 6(b)**. From the plot, it is clear that the hole-opening instability occurs mostly in the outer regime of the spreading.

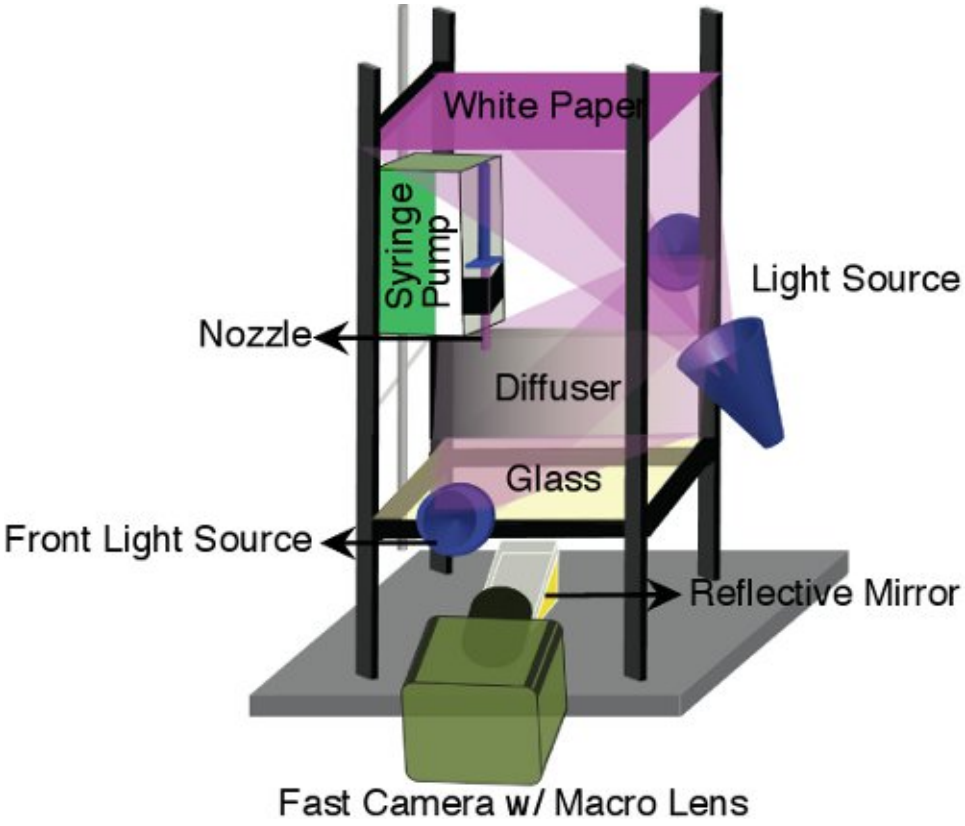


**Figure 1. Schematic illustration of the imaging setup**. The fast camera used for this work can achieve 6,242 frames-per-second (fps) at 1,280 x 800 widescreen resolution; the maximum frame rate is $10^6$ fps at reduced resolution (128 x 8). During the experiment, the drops were slowly extruded from a nozzle by using a syringe pump. The lighting of the system is provided by two white light sources. The front and back lights are used for liquid metal and dense suspension impact, respectively.

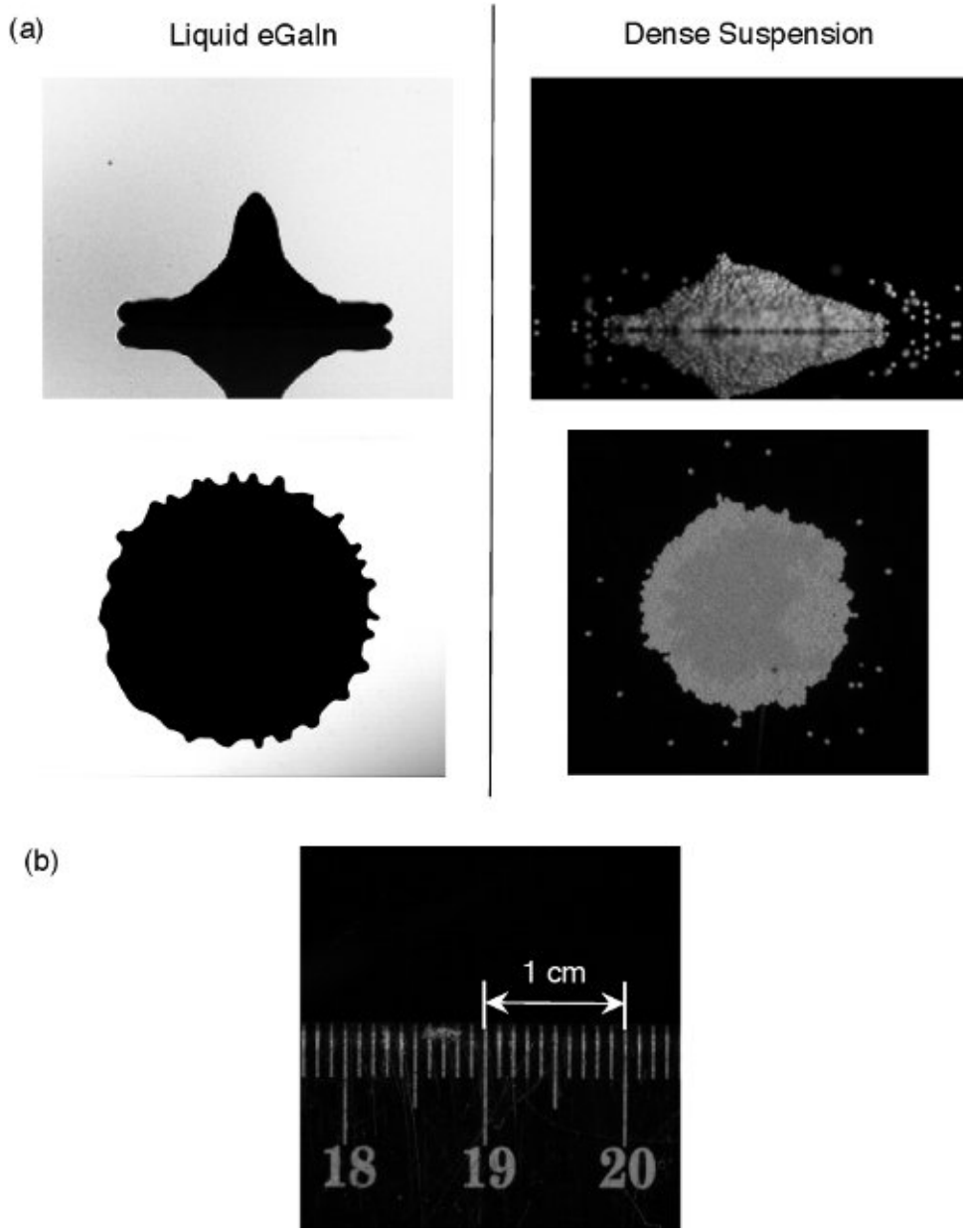


**Figure 2. (a) Typical Images taken by the camera for liquid eGaIn (left column) and a dense suspension of particles in a liquid (right column).** Observation can be performed from both bottom and side. To highlight the object's profile, the drop is illuminated in a direction perpendicular to the image plane. Specifically, for liquid eGaIn, the drop is backlit to increase the contrast at the liquid/air boundary. For dense suspensions, the sample is lit from the front, such that single particles in the drop can be distinguished. **(b)** An example of spatial resolution calibration at 10,000 fps. Here, there are 192 pixels across a distance of 1 cm. Thus, the spatial resolution for this figure is 1 cm/192 pixels ≈ 52 μm/pixel. Please click here to view a larger version of this figure.

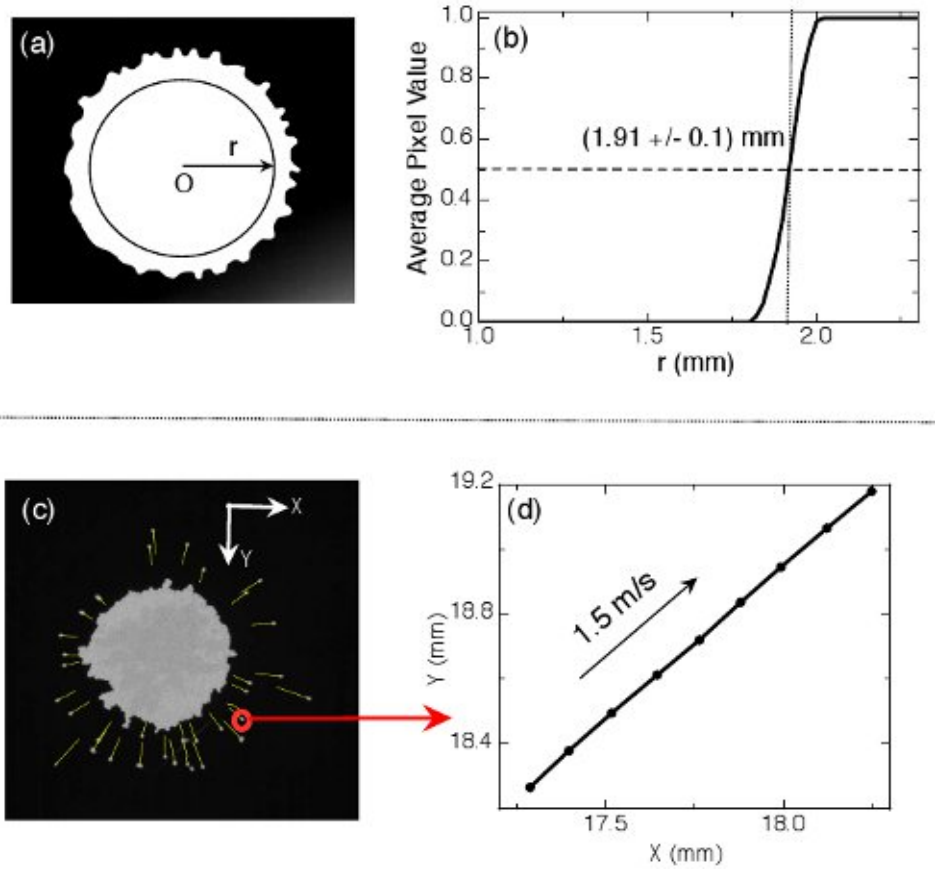


**Figure 3. Image Analysis.** For liquid metal drops, we first threshold the images for each frame (see **(a)**). The average pixel value along a ring at radial position r (see the solid circle in **(a)**) indicates the location of the spreading boundary. Conventionally, white corresponds to zero and black to one. As a result, the plot of average pixel value **(b)** shows a sharp transition. The position corresponding to 0.5 gives location of the boundary, where the uncertainty is coming from the width. The moving front is the key parameter for the study of spreading. By contrast, for dense suspension impact, not only the spreading but also the splashing onset is of concern. Panel **(c)** shows the result from particle tracking of splashing particles, where the yellow tails attached to the particles indicate their trajectories. The plot in **(d)** gives the trace of particles circled in **(c)**. Since the time step is 1/10,000 sec, the escaping velocity is constant at about 1.5 m/sec, which corresponds well to the impact velocity. Please click here to view a larger version of this figure.

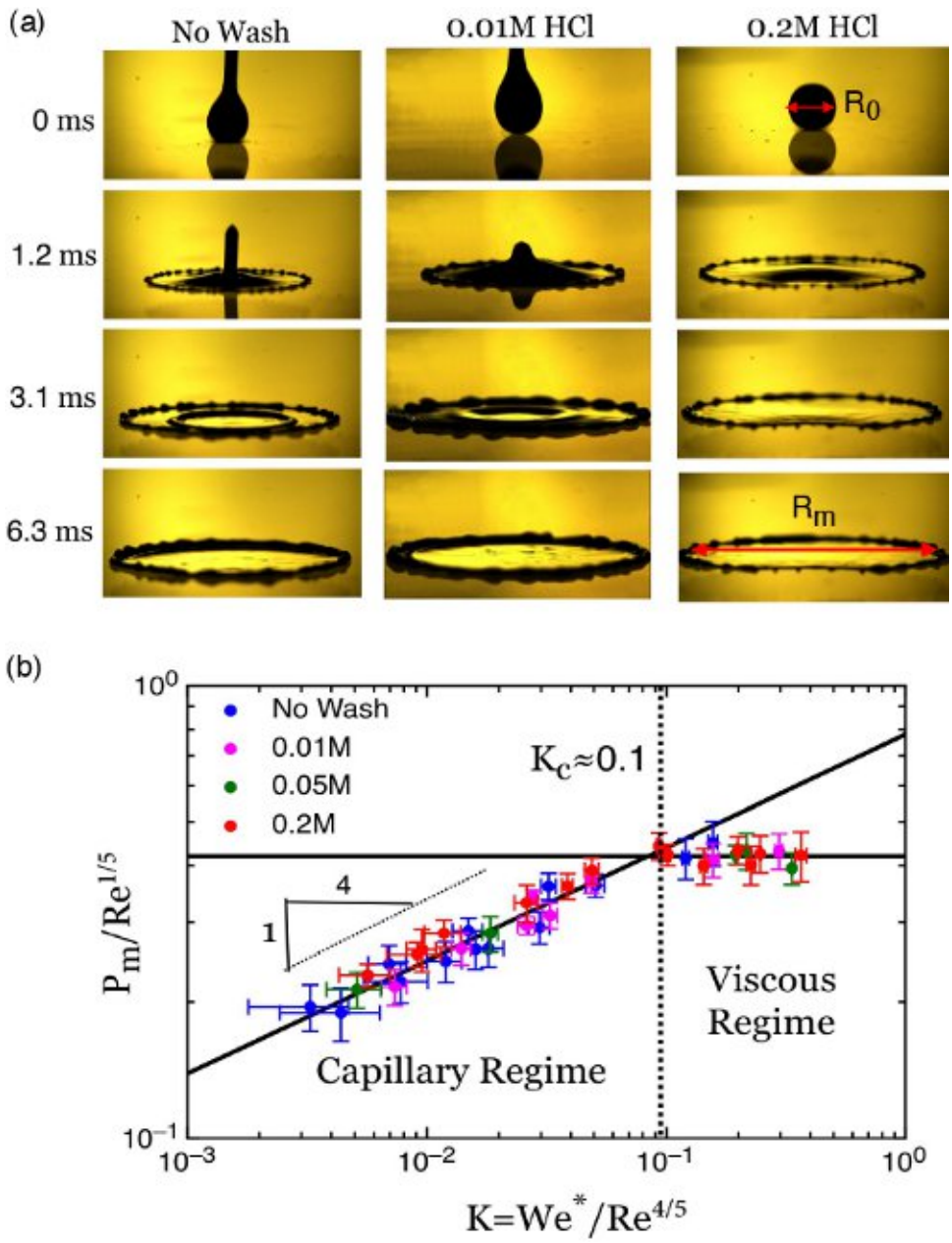


**Figure 4. Spreading dynamics of liquid eGaIn. (a)** Typical image sequence of eGaIn drops impacting onto a glass substrate (captured by a color-sensitive fast camera. In this case, the spatial resolution is reduced to 59 μm/pixel at 7,600 fps). Drops are initially prewashed in HCl solution as indicated in the text. For all image sequences shown above, the impact velocity was kept at $V_0$ = 1.02±0.12 m/sec and the initial drop diameter was $R_0$ = 6.25±0.10 mm. **(b)** Capillary to viscous transition for impact behavior of eGaIn drops prewashed with different acid concentrations. The dimensionless parameter $K=We^*/ Re^{4/5}$ is used to collapse all the data. Please click here to view a larger version of this figure.

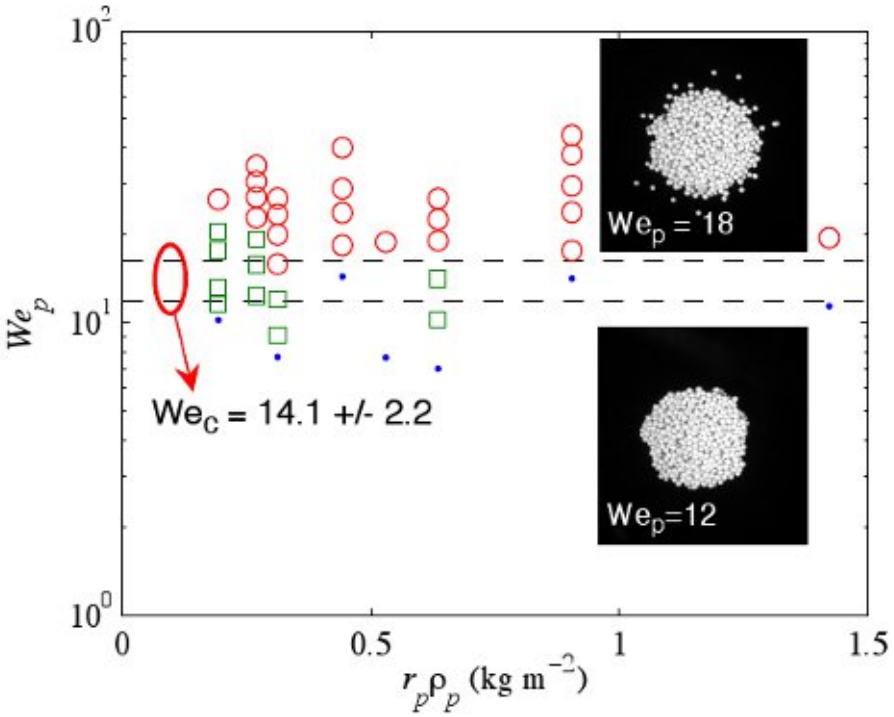


**Figure 5. Splash onset Weber number $We_p$ as a function of particle radius $r_p$ and density $\rho_p$.** The red hollow circles are the cases where splash is always found, and the solid blue dots correspond to the situation when no splash is found in 10 successive repeats. The open green squares indicate the scenarios when both splash and no splash are observed in the 10 repeats. The inset plots are typical images of splashing and nonsplashing cases. Please click here to view a larger version of this figure.

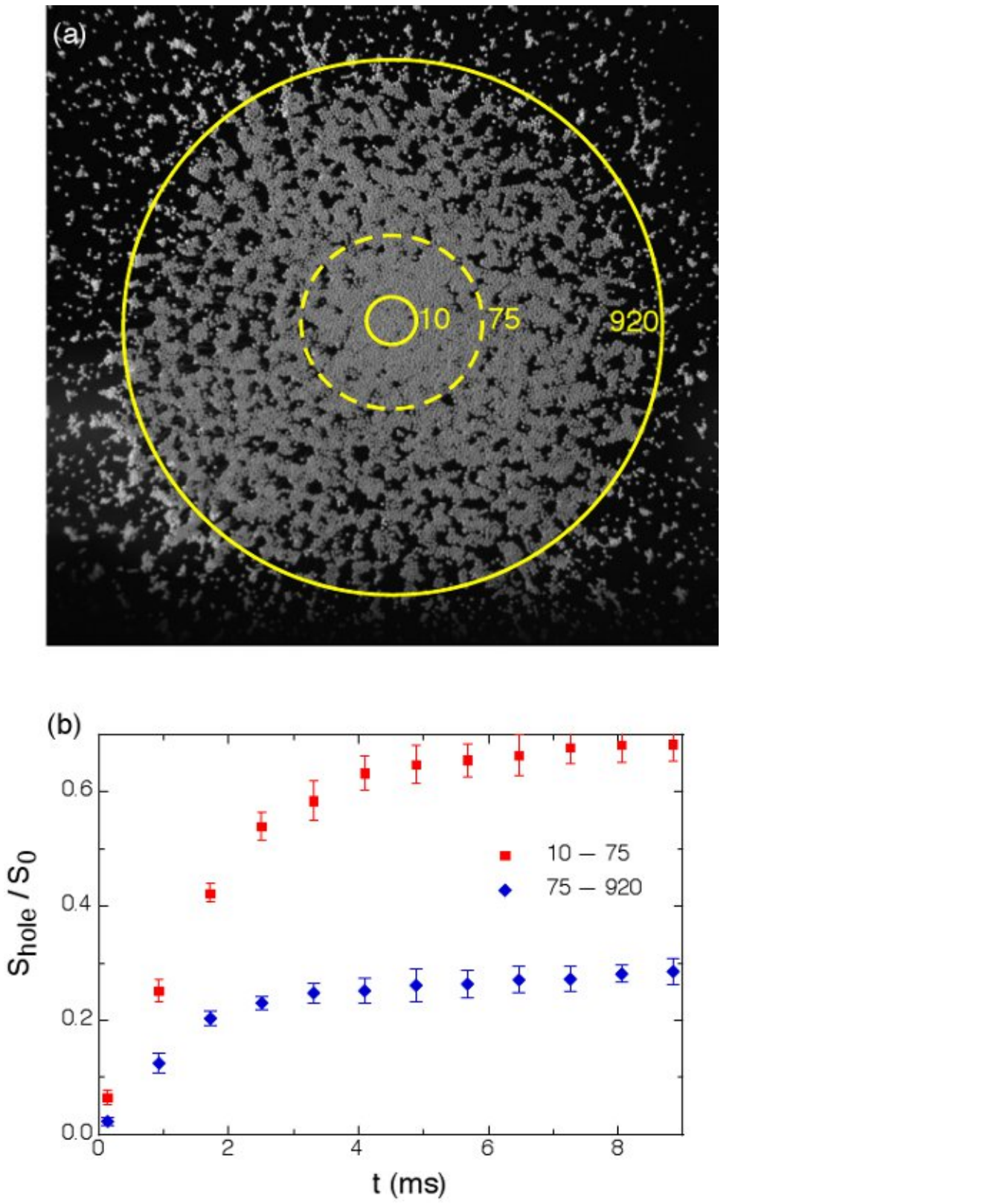


**Figure 6. Instability in suspension spreading dynamics.** Panel **(a)** shows a typical image during the impact. During spreading, holes open between particle clusters due to the velocity gradient in the monolayer. The three yellow rings in the image indicate the radial positions corresponding to different particle Weber numbers ($We_p$=10, 75, 920). **(b)** The ratio of the area of holes ($S_{hole}$) to the total area ($S_0$) between each ring. $S_{hole}/S_0$ is plotted against time, t.

## Discussion

Several steps are critical for proper execution of the fast imaging. First, camera and lens have to be appropriately set up and calibrated. In particular, in order to get high spatial resolution, the reproduction ratio of the lens must be kept close to 1:1. This is especially important for the visualization of dense suspensions. Also, the aperture size needs to be carefully chosen for imaging. For instance, observation from the side in general requires a longer depth of field, therefore smaller aperture size. To maintain the brightness of the video, one needs to increase the exposure time and thus reduce the frame rate (~6,000 fps). By contrast, bottom view only requires the camera to focus on one single plane. As a consequence, higher time resolution can be obtained (~10,000 fps).

Second, proper lighting setup is a key factor for getting a sharp boundary of the drops. Since all of the samples were lighted either from the back or front, the light sources need to be aligned vertically to the image plane. If the lighting angle is tilted, the shadow in the image and the surface reflection from the sample (*e.g.* from shiny surfaces such as liquid metals) can make accurate boundary detection impossible.

Third, the camera triggering is important when video recording. Users have to estimate how many frames should be recorded before triggering. The specific setup may vary with individuals, depending on different reaction times. Thus, several trial tests for practicing are necessary before actual measurements.

One limitation involves a spatial resolution trade-off. For most images taken in the experiments, the resolution was around 50 μm, which suggests that it is rather difficult to clearly visualize particles smaller than 50 μm (although advanced particle tracking algorithms might help in this regard, depending on the specific experimental details[10-12]). Another potential limitation is the sharp reduction in time resolution when the required field of view becomes large. For the splat extending to several centimeters, the frame rate can drop below 5,000 fps, which may not be quick enough for capturing fast dynamics.

In summary, the fast imaging system (fast camera + macro lens) described here is a promising tool for studying fast dynamics processes. The focus here was on impact of non-Newtonian fluids, but investigations of many other research topics, such as liquid drop breakup[19,20], granular jets[21], and liquid drop coalescence[22], benefit from a similar technique. Such experimental approach makes it possible to image microscale phenomena and at the same time obtain insights into the accompanying dynamics at the scale of microseconds, a regime that is challenging for conventional imaging methods.

## Disclosures

The authors have nothing to disclose.

## Acknowledgements

Thanks to Wendy Zhang, Luuk Lubbers, Marc Miskin and Michelle Driscoll for many useful discussions and Qiti Guo for help with preparing experimental samples. This work was supported by the National Science Foundation's MRSEC program under Grant No. DMR-0820054.

## References

1. Chiechi, R. C., Weiss, E. A., Dickey, M. D., and Whitsides, G. M. Eutectic Gallium-Indium (EGaIn): A moldable Liquid Metal for Electrical Characterization of Self-Assembled Monolayers. *Angew. Chem. Int. Ed.* **47**, 142 (2008).
2. Fukumoto, M. and Huang, Y. Flattening Mechanism in Thermal Sprayed Ni Particles Impinging on Flat Substrate Surface. *J. Thermal Spray Tech.* **8**, 427 (1999).
3. Seerden, K. A., Reis, N., Evans, J. R., Grant, P. S., Halloran, J. W., and Derby, B. Ink-Jet Printing of Wax-Based Alumina Suspensions. *J. Am. Ceram. Soc.* **84,** 2514 (2004).
4. Derby, B. Inkjet printing ceramics: From drops to solid. *J. Eur. Ceram. Soc.* **31,** 2543 (2011).
5. Xu, L., Zhang, W. W., and Nagel, S. R. Drop Splashing on a Dry Smooth Surface. *Phys. Rev. Lett.* **94**, 184505 (2005).
6. Clanet, C., Beguin, C., Richard, D., and Quere, D. Maximal deformation of an impacting drop. *J. Fluid. Mech.* **517,** 199 (2004).
7. Yarin, A. L. Drop Impact Dynamics: Splashing, Spreading, Receding, Bouncing. *Annu. Rev. Fluid Mech.* **38,** 159 (2006).
8. Chandra, S. and Avedisian, C. T. On the collision of a droplet with a solid surface. *Proc. R. Soc. Lond. A* **432**, 13-41 (1991).
9. Versluis, M. High-speed imaging in fluids. *Exp. Fluids.* **54**, 1458 (2013).
10. Thoraval, M.-J., Takehara, K., Etoh, T. G., and Thoroddsen, S. T., Drop impact entrapment of bubble rings*, J. Fluid Mech*. **724,** 234-258 (2013).
11. Thoroddsen, S. T., Takehara, K., and Etoh, T. G., Micro-splashing by drop impacts, *J. Fluid Mech*. **706**, 560-570 (2012).
12. Thoroddsen, S. T., Etoh, T. G., and Takehara, K., High-speed imaging of drops and bubble, *Ann. Rev. Fluid Mech*. **40**, 257-285 (2008).
13. Driscoll, M., Stevens, C. S., and Nagel, S. R. Thin film formation during splashing of viscous liquids. *Phys. Rev. E.* **82**, 036302 (2010).
14. Pregent, S., Adams, S., Butler, M. F., and Waigh, T. A. The impact and deformation of a viscoelastic drop at the air-liquid interface. *J. Non-Newtonian Fluid Mech.* **166**, 831 (2011).
15. Xu, Q., Brown, E., Jaeger, H. M. Impact dynamics of oxidized liquid metal drops. *Phys. Rev. E.* **87**, 043012 (2013).
16. Peters, I. R., Xu, Q., Jaeger, H. M. Splashing onset in dense suspension droplets. *Phys. Rev. Lett.* **111**, 028301 (2013).
17. Luu, L., Forterre, Y. Drop impact of yield-stress fluids. *J. Fluid Mech.* **632**, 301 (2009).
18. Xu, Q., Oudalov, N., Guo, Q., Jaeger, H., and Brown, E. Effect of oxidation on the mechanical properties of liquid gallium and eutectic gallium-indium. *Phys. Fluids.* **24**, 063101 (2012).
19. Turitsyn, K. S., Lai, and L., Zhang, W. W. Asymmetric Disconnection of an Underwater Air Bubble: Persistent Neck Vibrations Evolve into a smooth Contact. *Phys. Rev. Lett.* **103**, 124501 (2009).

 

20. Miskin, M. Z. and Jaeger, H. M. Droplet Formation and Scaling in Dense Suspensions. *Proc. Natl. Acad. Sci. U.S.A.* **109**, 4389-4394 (2012).
21. Royer, J. R., *et al.* Birth and growth of a granular jet. *Phys. Rev. E.* **78,** 011305 (2008).
22. Paulsen, J. D., Burton, J. C., Nagel, S. R. Viscous to Inertial Crossover in Liquid Drop Coalescence. *Phys. Rev. Lett.* **106**, 114501 (2011).

 